RESEARCH ARTICLE | FEBRUARY 27 2019

Thermal management with a highly emissive and thermally conductive graphite absorber

Tingbiao Guo; Yaoran Sun ■ (D); Julian Evans (D); Nan Wang; Yang Fu; Sailing He



AIP Advances 9, 025224 (2019) https://doi.org/10.1063/1.5086064





Articles You May Be Interested In

Theoretical analysis of solar cell performance assisted by passive cooling

Appl. Phys. Lett. (September 2025)

Carbon nanotube-based black coatings

Appl. Phys. Rev. (February 2018)

Patterning of graphite nanocones for broadband solar spectrum absorption

AIP Advances (June 2015)





Thermal management with a highly emissive and thermally conductive graphite absorber

Cite as: AIP Advances 9, 025224 (2019); doi: 10.1063/1.5086064 Submitted: 17 December 2018 • Accepted: 19 February 2019 • Published Online: 27 February 2019







Tingbiao Guo, ^{1,a)} Yaoran Sun, ^{1,a),b)} D Julian Evans, ¹ Nan Wang, ¹ Yang Fu, ¹ and Sailing He^{1,2}

AFFILIATIONS

- ¹Centre for Optical and Electromagnetic Research, College of Optical Science and Engineering, Zhejiang University, Hangzhou 310058, People's Republic of China
- ²Department of Electromagnetic Engineering, Royal Institute of Technology, S-100 44 Stockholm, Sweden
- a) Contributions: Tingbiao Guo and Yaoran Sun contributed equally to this work.
- b) Author to whom correspondence should be addressed: sunoi@zju.edu.cn

ABSTRACT

Thermal management on a variety of length scales is essential for many industrial, solar and computational systems. Here we explore the thermal properties of a nearly perfect graphite absorber with both high emissivity and thermal conductivity which is fabricated by simple one-step etching. The hemispherical reflectance of the absorber is around 1% in the visible range and the normal specular reflectance is less than 1% from 1.5 μ m to 10 μ m. The thermal conductivity of the absorber is measured above 630 Wm⁻¹K⁻¹, which is 2.5 times larger than the aluminum used in commercial heat sinks. Heat dissipation testing indicates that a device is 3.7 \pm 2 degrees cooler with the graphite absorber as the heat spreader than a pristine graphite sheet and 9.1 \pm 2 degrees cooler than an Au-coated graphite sheet, primarily due to improved radiation cooling. A theoretical analysis accounts for the results. Further analysis suggests that the radiative heat dissipation is more prominent in the low-convection environment, especially for a convection coefficient below 10 Wm⁻²K⁻¹.

© 2019 Author(s). All article content, except where otherwise noted, is licensed under a Creative Commons Attribution (CC BY) license (http://creativecommons.org/licenses/by/4.0/). https://doi.org/10.1063/1.5086064

I. INTRODUCTION

Thermal management is a crucial subject for both consumer electronics and industrial electronics. High temperature can increase the power consumption and hinder the performance of the device. Studies suggest that decreasing the setpoint temperature by only one degree in a data center can lead to a reduction of the power consumption by 2-5%. There are three primary mechanisms for heat transfer: thermal conduction, thermal convection and thermal radiation. The thermal radiation power is proportional to the emissivity of the surface. According to Kirchhoff's radiation law, the emissivity of an arbitrary body is equal to its absorptivity at thermodynamic equilibrium, which means a perfect absorber is also a good heat dissipation material.² Since a room temperature blackbody's radiation has a peak around 10 microns, broadband ultra-black materials (from VIS to mid-IR) are efficient for radiative heat transfer³ especially in natural convection and low-airflow applications. Carbon can be an ideal black material for thermal management among various platforms due to its high absorption and excellent

thermal quality. Vertically aligned carbon nanotube arrays (VANTA) are the best-known material for approaching perfect absorption.⁴ They have been used to get an ultra-black absorber across a wide spectral range from UV (200 nm) to far infrared (200 µm) with the reflectance well below 1%. Other ultra-black absorbers based on highly ordered pyrolytic graphite (HOPG),⁵ carbon-based coating⁶ and carbon-coated black silicon⁷ also show extremely high absorption in the visible to near-infrared region. Thermal conduction is also an important heat transfer mechanism in portable electronics, especially for thermal homogenization. But for most ultra-black materials, the thermal conductivity is restricted to the region below 100 Wm⁻¹K⁻¹,⁸⁻¹¹ which limits their applications for heat transfer. Copper and aluminum are mostly used materials for thermal dissipation due to their large thermal conductivity (401 Wm⁻¹K⁻¹ and 237 Wm⁻¹K⁻¹ respectively). Other materials with thermal conductivity above 1000 Wm⁻¹K⁻¹ such as graphitized polyimide film, ¹² graphene fibers, ¹³ graphene sheets ^{14–17} have also been produced. But to meet the challenge of thermal dissipation in compact electronics, it is urgent to obtain a material with

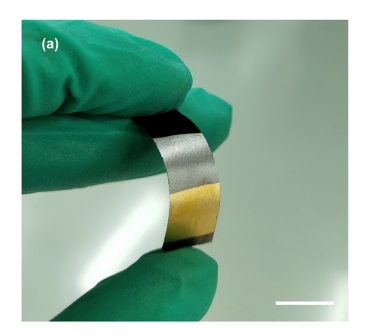
both high thermal conductivity and high emissivity as a thermal

In this paper, we report the cooling properties of nearly perfect absorber with high emissivity and thermal conductivity produced from a commercially available synthetic graphite sheet (Panasonic Corporation). This broadband (from VIS to mid-IR) graphite absorber can be fabricated easily by a one-step etching process. The graphite sheet itself is flexible, light-weight and has excellent thermal conductivity in the range from 700-1950 Wm⁻¹K⁻¹.18 Combining the high emissivity and thermal conductivity, the ultrablack graphite absorber (UGA) can be an attractive option for various thermal applications such as mobile phone and wearable electronics.

II. EXPERIMENT AND RESULTS

The graphite absorber made from graphite sheet (35 mm \times $10 \text{ mm} \times 25 \text{ } \mu\text{m}$) was fabricated by oxygen-plasma etching in an inductively coupled plasma reactive ion etching (ICP-RIE) system. The sample was placed on a silicon wafer holder which provided the nanoparticle masks responsible for the formation of the structures. The reactive gas was pure oxygen (O2) with a typical flow rate of 90 sccm. The ICP RF power and the RIE RF power were 100 W and 300 W respectively. The etching time was 10, 20, 30 and 60 minutes with a fixed chamber pressure of 30 mTorr (labeled as UGA-10, UGA-20, UGA-30, and UGA-60, respectively). Fig. 1 shows the photograph and SEM picture of a UGA. Pillar-like structures are formed on the surface. These structures on the graphite sheet are due to the self-mask effect where silicon nanoparticles are sputtered from the substrate onto the carbon as we have described in detail elsewhere. 19 After 60-minutes etching, the height of the pillars can be up to 9 μ m. According to the effective medium theory, this textured surface will cause a gradient refractive index between the graphite sheet and the air boundary. As a result, impedance mismatch will be diminished and the reflection will be suppressed following Fresnel's law.

The absorptivity of A = 1 - R - T, where R is the reflectivity and T is the transmittivity. So we characterize the absorptivity by measuring the reflectivity and transmittivity. We used the Ocean Optics STS-VIS spectrometer mounted with an integrating sphere ISP-REF to measure the hemispherical (specular and diffuse) reflectance from 450 nm to 850 nm. The reflectance was normalized to a standard whiteboard. In the mid-infrared region, a Bruker VERTEX 70 Fourier transform infrared (FTIR) spectrometer on an unpolarized light source was used to measure the specular reflectance with a gold mirror as the reference. The normal incident reflectance was measured with a 15× objective with NA = 0.4. Fig. 2 shows the total hemispherical reflectance and normal specular reflectance for different absorbers in the VIS and IR region. As we can see, the reflectances remain around 1% for UGA with etching time above 20 minutes in the VIS region. Meanwhile, in the IR regime, the reflectance decreases as the etching time increases. This is caused by the different height of the nanopillars on the graphite surface. The nanopillars will get denser and higher on the sheet surface with the etching time increasing (from several hundred nanometers to several micrometers). Following by the decreasing of the material density on the surface, the electron density and therefore the permittivity will decrease.²⁰ As a result, the refractive index of the device will get closer to 1 on the air-graphite boundary. When the wavelength



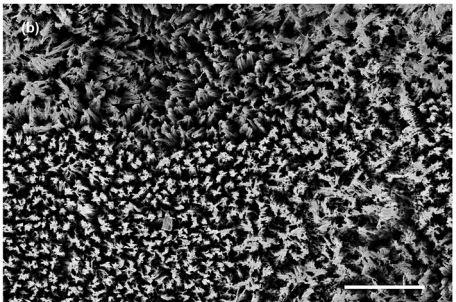


FIG. 1. (a) A photograph of flexible graphite sheet with various reflectivity. From top to bottom: etched graphite, pristine graphite and Au-coated graphite. (b) A tilted SEM picture of the as-prepared absorber which shows needle-like structures. Scale bar: 1 cm in (a) and 10 µm in (b).

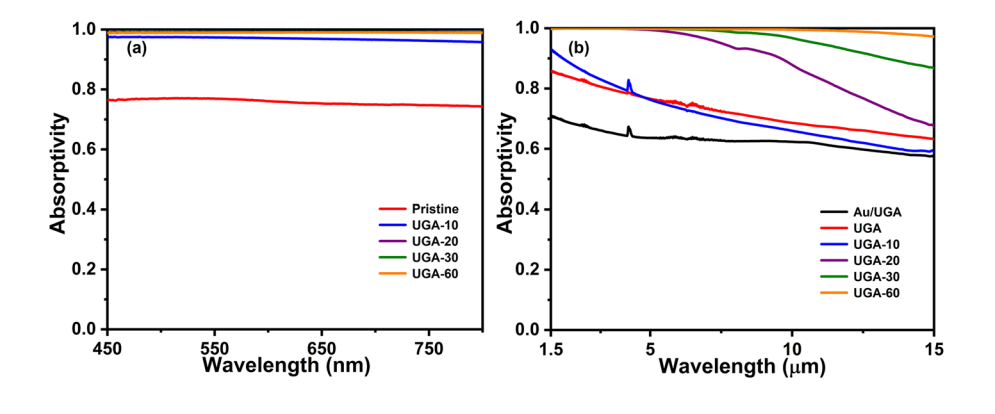


FIG. 2. (a) The measured total hemispherical absorptivity of our absorbers in the visible range. (b) The measured normal specular reflectivity of the absorbers in the IR region.

TABLE I. The thermal diffusivity, density and thermal conductivity for different graphite absorbers.

	UGA-10	UGA-20	UGA-30	UGA-60
$\alpha (\text{mm}^2 \text{s}^{-1})$	772.6	828.0	843.7	858.9
ρ (gcm ⁻³)	1.77	1.67	1.49	1.37
k_{eff} (Wm ⁻¹ K ⁻¹)	737	745	678	634

is larger than the size of the pillars, effect refractive index will increase so as the reflectance. The reflectance can reach below 1% in the range from 0.45 μ m to 10 μ m for UGA-60, which is comparable to the VANTA material in the same region. Further measurement (not shown in the paper) in the IR region shows no transmission for our absorbers. So the emissivity is $\varepsilon = A = 1 - R$ for all absorbers. The different reflectances indicate that we can tune the emission of our absorbers by controlling the etching time (see Fig. 1(b)).

These absorbers have relatively high thermal conductivity among the ultra-black materials. 8-11 To ensure the thermal conductivity (k) of UGA, the laser flash method (Netzsch LFA 467)²¹ was used to get the thermal diffusivity (α). Then the effective thermal conductivity is calculated using Equation: $k_{eff} = \alpha \rho C_P$, where ρ is the density of the sample, which is obtained by mass divided by volume. Here we assume the thickness is 25 µm for all absorbers, though plasma etching will thin the sheet. So the actual density is larger than the calculated number and so as the thermal conductivity. C_P is the specific heat capacity obtained from differential scanning calorimetry (TA Q200) and is measured as 0.593 Jg⁻¹°C⁻¹ at 25 °C. Table I shows α , ρ and k_{eff} for different samples.

The results indicate the effective thermal conductivity of our absorbers can be higher than $634~\rm Wm^{-1}\,K^{-1}$, which is 2.5 times larger than aluminum which is commonly used for thermal management. Considering the high emissivity and high thermal conductivity, it is expected these absorbers can be used for heat dissipation. To demonstrate the role of radiative thermal dissipation of these perfect absorbers, a control experiment was conducted. In the experiment, three graphite sheets with low, medium and high emissivity were used as a heat spreader. To get a low-emissivity graphite sheet, we sputtered a thick gold layer (100 nm) on the pristine graphite sheet. The pristine (also sputtered a 100 nm gold layer underneath the sheet for comparison) and UGA-60 graphite sheet were used as

medium- and high-emissivity heat spreaders respectively. The emissivity of the Au-coated graphite sheet, pristine graphite sheet and UGA-60 sheet are shown in Fig. 2.

The inset in Fig. 3(a) shows the schematic configuration for the experiment. A polyimide (PI) heater (1.2 cm × 3.9 cm) was used to heat a silicon plate. The UGA-60, pristine graphite sheet and Aucoated graphite sheet were attached to the plate with silver paste, respectively. A T-type temperature monitor with accuracy ± 1 °C was placed on the surface of the silicon plate to detect the temperature change. The device was placed on a styrofoam and the whole device was placed in a PMMA box to maintain the identical environment for all experiments. By varying the input current to the heater, the temperature of the silicon plate was measured at steady-state. Fig. 3(c) shows the measured temperature change as a function of input power. Compared to the one with Au-coated graphite sheet, silicon plate is 5.4 ± 2 °C cooler with pristine graphite sheet and 9.1± 2 °C cooler with UGA-60 at around 80 °C. This is a great enhancement as the reliability of circuits is exponentially dependent on the operating temperature of the device. Higher temperature will dramatically hinder the performance of electronics. In the experiment, as all graphite pristine sheets have similar thickness and both thermal conductivities are much larger than air, the effective convection and conduction coefficient can be treated as the same in all experiments. So the temperature decrease is mainly caused by the radiation effect as the emissivity of UGA-60 and pristine graphite sheet are larger than the Au-coated graphite sheet.

To better understand the mechanism for the temperature difference in the experiments, a simple model can be applied to explain the results. According to the conservation of energy principle, the total input power is equal to the output power for an object at steady state. In our case, the output power (P_{loss}) is composed of radiation loss (P_{rad}) and nonradiation loss (convection and conduction loss, P_{nonrad}). The total heat loss power can be written as $P_{loss} = P_{rad} + P_{nonrad}$. And the total input power can state as:

$$P_{in} = P_e \eta = P_{rad} + P_{nonrad} \tag{1}$$

Here P_e means the input electric power and can be calculated as $P_e = I^2 R$. η means the efficiency of the electro-thermal conversion.

For an object at temperature T, the radiation power can be determined by the Planck's law:

$$P_{obj} = A \int d\Omega cos\theta \int_0^\infty \frac{2hc^2}{\lambda^5} \frac{1}{e^{\frac{hc}{\lambda k_B T}} - 1} \varepsilon(\lambda, \theta) d\lambda$$
 (2)

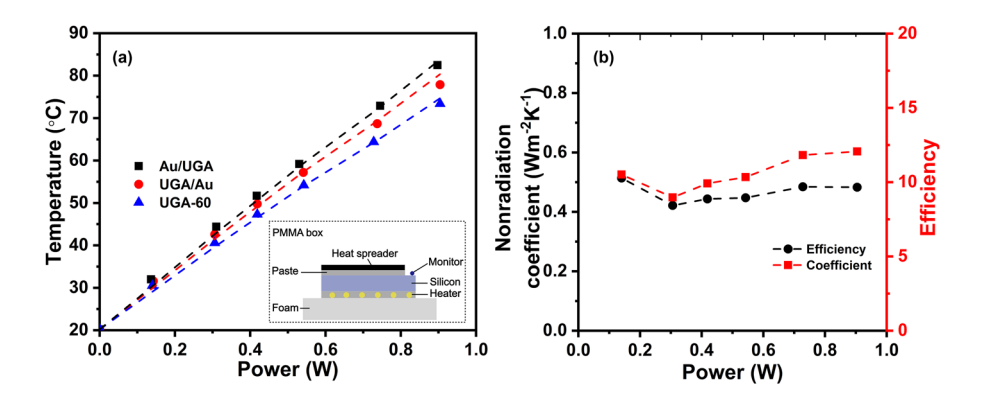


FIG. 3. (a) The measured steady-state temperature change as a function of input power. Square for Aucoated pristine graphite sheet, circle for pristine sheet and triangle for the UGA-60 absorber. Inset: the schematic setup for heat dissipation experiment. (b) The power conversion efficiency η and the nonradiation coefficient h_{nonrad} calculated from experimental results.

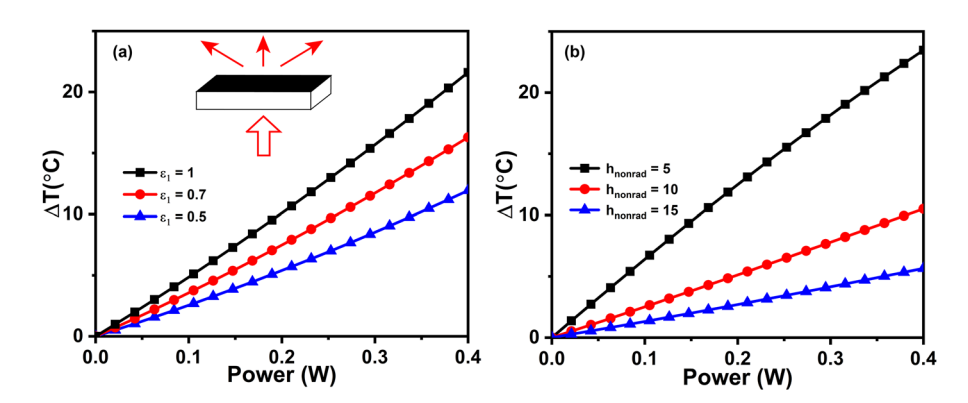


FIG. 4. (a) The calculated temperature difference for three emissivities (UGA-60, pristine graphite sheet and Au-coated graphite) with different input power. ε_2 is set to be 0.1. h_{nonrad} is set to be 10.6 Wm⁻²K⁻¹. Inset: an object with a radiative heat spreader. (b) The calculated temperature difference for various nonradiation coefficient with different input power. ε_2 and ε_1 are set to be 0.5 and 1 respectively.

Here A is the surface area of the object. $\int d\Omega = 2\pi \int_0^{\pi/2} d\theta sin\theta$ is the angular integral over a hemisphere. h is Planck's constant, k_B is the Boltzmann constant, c is the speed of light, λ is the wavelength and $\varepsilon(\lambda,\theta)$ is the emissivity of the object. The net radiation loss power is the difference between the object and air radiation power. Assuming the emissivity of the object is a constant over a hemisphere, the radiation loss power of the object can be written as:

$$P_{rad} = A\pi \left(\int_0^\infty \frac{2hc^2}{\lambda^5} \frac{1}{e^{\frac{hc}{\lambda k_B T}} - 1} \varepsilon(\lambda) d\lambda - \int_0^\infty \frac{2hc^2}{\lambda^5} \frac{1}{e^{\frac{hc}{\lambda k_B T_0}} - 1} \varepsilon(\lambda) d\lambda \right)$$
(3)

For the nonradiative effect, heat dissipation power can be written as:

$$P_{nonrad} = Ah_{nonrad}(T - T_0) \tag{4}$$

Here h_{nonrad} is the effective heat coefficient for convection and conduction.

In our experiment, the emissivities of three graphite sheets can be determined from Fig. 2 for wavelengths between 1.5 μ m and 15 μ m. The areas covered by the heat spreader and the total area of the device in the air are 3.5×10^{-4} m² and 4.9×10^{-4} m² respectively. The resistance of the heater in our experiment is 30 Ω . The room temperature T_0 is measured around 20.2 °C. Here we assume η and h_{nonrad} are same in all experiments for the same input power. Using Eq. (1), (3), (4), we can solve η and h_{nonrad} shown in Fig. 3(b). η and h_{nonrad} are around 0.47 and 10.6 Wm $^{-2}$ K $^{-1}$ respectively. Low energy conversion efficiency is mainly due to the resistance of the wire. h_{nonrad} is comparable with the natural convection coefficient of air and increases as the input power increases. This is reasonable as higher input power will cause a higher temperature difference and consequently enhance the air-flow, so as the nonradiation coefficient.

To verify the validity of our model, we calculated the emissivity for the Au-coated graphite sheet. The calculated emissivity is ~ 0.15 smaller than the measured one. This result is ambiguous as the scattering of the gold surface is pretty severe while the NA of the objective used for measuring the reflection (emission) is only 0.4. We measured the reflection of Au-coated graphite sheet with different NA objectives in visible region. It shows that the reflection is ~ 0.3 for NA = 0.3 and ~ 0.8 for NA = 0.9. Using the average emissivity of three sheets and average η and h_{nonrad} , we fit the experimental

data with our model. Fig. 3 shows the calculated results and these calculated results fit well with measured ones.

In order to investigate the influence of emissivity and the nonradiative coefficient to heat dissipation, we do some simulations in which an object with a thin radiative heat spreader sheet on it is considered (see inset in Fig. 4(a)). All the parameters are the same with the experiment. The total area of the object and the spreader are set to be 4.9×10^{-4} m² and 3.5×10^{-4} m². The initial temperature is set to be 20.2 °C. And the emissivity ε_2 is assumed to be equal to the Al spreader and is set to be 0.1. Temperature difference ($\Delta T = T_2 - T_1$) is calculated for spreaders with emissivity ε_1 and ε_2 by varying input power. Fig. 4 shows the ΔT change as a function of input power with various ε_1 and h_{nonrad} . As can be seen from Fig. 4(a), for a constant nonradiation coefficient (10.6 Wm⁻²K⁻¹), the higher the emissivity of the heat spreader, the better the heat dissipation performance. And the temperature difference increases with the input power as the radiation effect is proportional to T^4 . The temperature can decrease ~20 °C for the input power around 0.4 W, as the emissivity increases from 0.1 to 1, which shows great superiority of our ultra-black absorber compared with metal-based heat spreader as aluminum and copper films are poor emitters in the infrared range. Moreover, for a constant $\Delta \varepsilon$ ($\varepsilon_1 = 1$ and $\varepsilon_2 = 0.5$), larger temperature difference will occur for smaller convection and conduction coefficient, especially for nonradiation coefficient less than 10 Wm⁻²K⁻¹. This shows our absorber is a promising candidate for heat dissipation application as the natural air convection coefficient is around 10 Wm⁻²K⁻¹.

III. CONCLUSIONS

In brief, we report an ultra-black graphite absorber with high emissivity and high thermal conductivity based on a commercially available graphite sheet. A simple self-masked etching process is introduced to fabricate the absorber and the emissivity can be tuned by changing the etching time. The results show the hemispherical reflectance of the absorber in the visible range is around 1% and the normal specular reflectance is below 1% in the range from 1.5 μm to 10 μm . Laser flash method confirms the thermal conductivity of the absorber is above 630 $Wm^{-1}K^{-1}$, which is 2.5 times higher than aluminum. Experiments indicate the absorber has a faster heat transfer than aluminum foil and better heat dissipation performance than pristine graphite sheet due to higher thermal conductivity

and emissivity. Combining flexibility, lightweight and high thermal conductivity, the ultra-black graphite absorber is a very promising candidate for thermal management, especially in the low-convection and low-airflow applications.

ACKNOWLEDGMENTS

We thank Jiang Yang for the help of reflectance measurement. This work was partially supported by the National Natural Science foundation of China (No. 61550110246, No. 91833303 and No. 11621101). Yaoran Sun proposed the idea for the paper. Tingbiao Guo conducted the experiment. Julian Evans, Nan Wang and Sailing He involved in the discussion and contributed to the manuscript. Yang Fu helped to measure the reflectance in IR region. Tingbiao Guo and Yaoran Sun contributed equally to this work.

REFERENCES

- ¹N. El-Sayed, I. A. Stefanovici, G. Amvrosiadis, A. A. Hwang, and B. Schroeder, ACM SIGMETRICS Performance Evaluation Review **40**(1), 163 (2012).
- ²J. R. Howell, M. Pinar Mengüç, and R. Siegel, *Thermal radiation heat transfer*, Sixth ed. (CRC Press, Boca Raton, FL, 2016).
- ³X. He, Y. Li, L. Wang, Y. Sun, and S. Zhang, Thin Solid Films **517**(17), 5120 (2009).
- ⁴Zu-P. Yang, L. Ci, J. A. Bur, S.-Y. Lin, and P. M. Ajayan, Nano Lett. 8(2), 446 (2008).
- ⁵Y. Sun, J. Evans, F. Ding, N. Liu, L. Wen, Y. Zhang, and S. He, Opt. Express 23(15), 20115 (2015).
- ⁶L. Zhao, X. He, J. Li, X. Gao, and J. Jia, Sensors and Actuators A: Physical **196**, 16 (2013)

- ⁷A. Shah, P. Stenberg, L. Karvonen, R. Ali, S. Honkanen, H. Lipsanen, N. Peyghambarian, M. Kuittinen, Y. Svirko, and T. Kaplas, Scientific Reports **6**(1), 25922 (2016).
- ⁸O. Raghu and J. Philip, Meas. Sci. Technol. **17**(11), 2945 (2006).
- ⁹S. Xie, W. Li, Z. Pan, B. Chang, and L. Sun, J. Phys. Chem. Solids **61**(7), 1153 (2000).
- ¹⁰I. Ivanov, A. Puretzky, G. Eres, H. Wang, Z. Pan, H. Cui, R. Jin, J. Howe, and D. B. Geohegan, Appl. Phys. Lett. 89(22), 223110 (2006).
- ¹¹ J.-H. Lee, J. C. Grossman, J. Reed, and G. Galli, Appl. Phys. Lett. **91**(22), 223110 (2007).
- ¹²B. Shen, W. Zhai, and W. Zheng, Adv. Funct. Mater. 24(28), 4542 (2014).
- ¹³ G. Xin, T. Yao, H. Sun, S. Michael Scott, D. Shao, G. Wang, and J. Lian, Science 349(6252), 1083 (2015).
- ¹⁴A. A. Balandin, S. Ghosh, W. Bao, I. Calizo, D. Teweldebrhan, F. Miao, and C. Ning Lau, Nano Lett. 8(3), 902 (2008).
- ¹⁵ A. A. Balandin, Nature Materials **10**(8), 569 (2011).
- ¹⁶H. Malekpour, K. H. Chang, J. C. Chen, C. Y. Lu, D. L. Nika, K. S. Novoselov, and A. A. Balandin, Nano Lett. 14(9), 5155 (2014).
- ¹⁷F. Kargar, Z. Barani, R. Salgado, B. Debnath, J. S. Lewis, E. Aytan, R. K. Lake, and A. A. Balandin, ACS applied materials & interfaces 10(43), 37555 (2018).
- 18 https://industrial.panasonic.cn/ea/products/thermal-solutions/graphite-sheet-pgs/pgs.
- ¹⁹T. Guo, Y. Sun, S. He, J. Yang, M. Hu, W. Mu, and J. Evans, Progress In Electromagnetics Research C 81, 191 (2018).
- ²⁰K. Mizuno, J. Ishii, H. Kishida, Y. Hayamizu, S. Yasuda, D. N. Futaba, M. Yumura, and K. Hata, Proceedings of the National Academy of Sciences 106(15), 6044 (2009).
- ²¹ L. Peng, Z. Xu, L. Zheng, Y. Guo, L. Peng, and C. Gao, Adv. Mater. 29(27), 1700589 (2017).